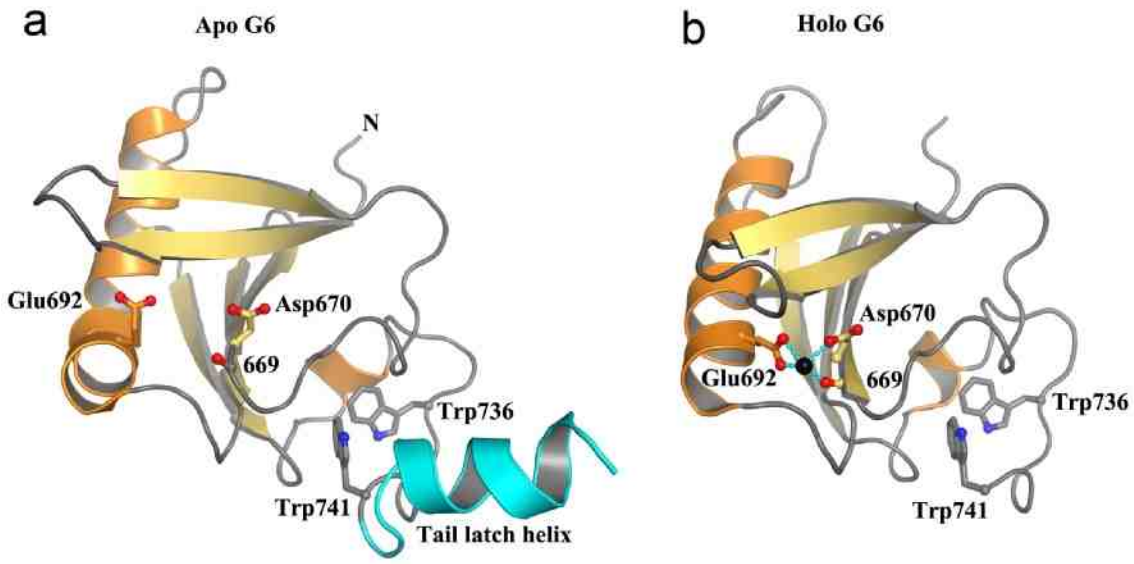

Supplementary Figure 1 Structures of apo and holo G6. (taken from: PDB ID 3FFN and PDB ID 1P8X, respectively). (a) Apo structure of G6. (b) Holo structure of G6. Since the C-terminal helix region is unstructured in the holo conformation, this region is not included in the holo G6 structure. The calcium ion binding coordination sphere (indicated by cyan dashes) of G6 is composed of the mainchain carbonyl oxygen from Asp669 and sidechain oxygens from Asp670 and Glu692. These residues adopt distinct positions in the apo versus the halo conformations. The calcium ion is shown in black. Trp741 from the C-terminal extension binds to G6 in both the apo and holo conformations. The C-terminal extension to G6 refers to residues 737-755. The truncated G6 (G6_cut) ends at Trp736. We speculate that Trp741 binding back to G6 influences the affinity of G6 for calcium and accounts for the differences in affinities of G6 and G6_cut. The C-terminal tail latch helix is coloured cyan. This region binds to G2 in the calcium-free conformation of whole gelsolin (not shown). N indicates the N-terminus of G6.

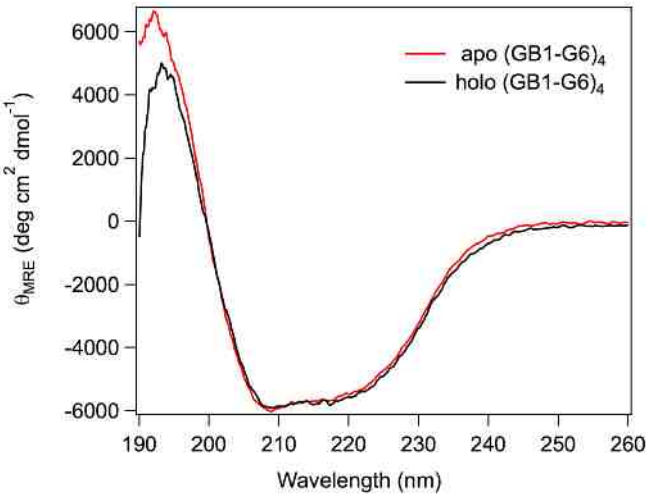

Supplementary Figure 2 Far-UV circular dichroism (CD) spectra of apo and holo G6. The CD spectra show a convolution of the signals from both GB1 and G6 and show the folded nature of the domains. The structural change on calcium binding to G6 cannot be detected by CD measurements.

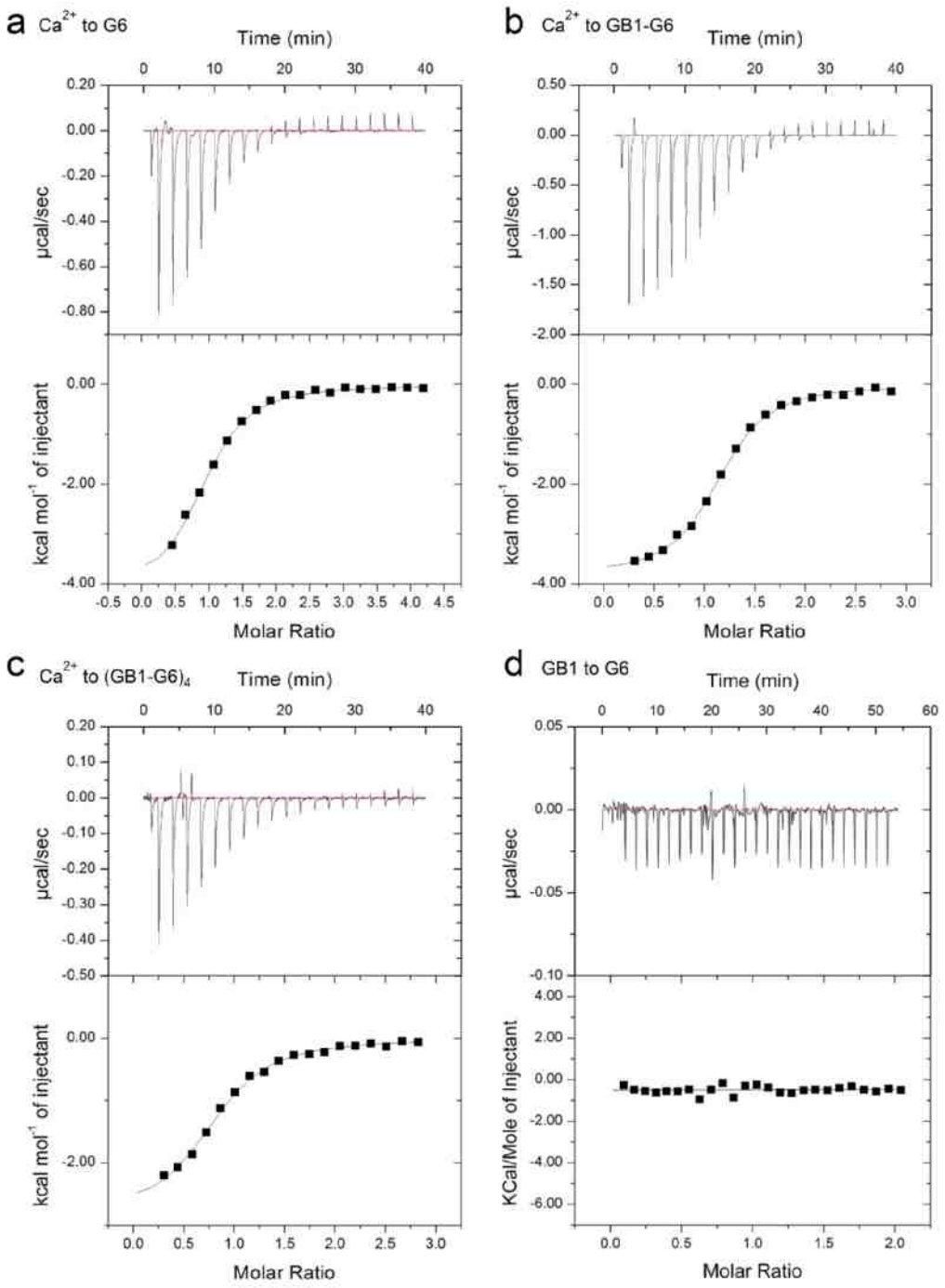

Supplementary Fig. 3 Isothermal titration calorimetry (ITC) measurement of the calcium dissociation constant (K_d) of G6. The experiments were done using different protein constructs (a, G6 monomer; b, GB1-G6; c, $(GB1\text{-}G6)_4$). The measured K_d values are 13.2 ± 1.6 µM, 12.1± 2.0 µM, and 14.4 ± 1.5 µM, respectively. (d) ITC measurements indicated that GB1 does not exhibit measurable binding to G6.

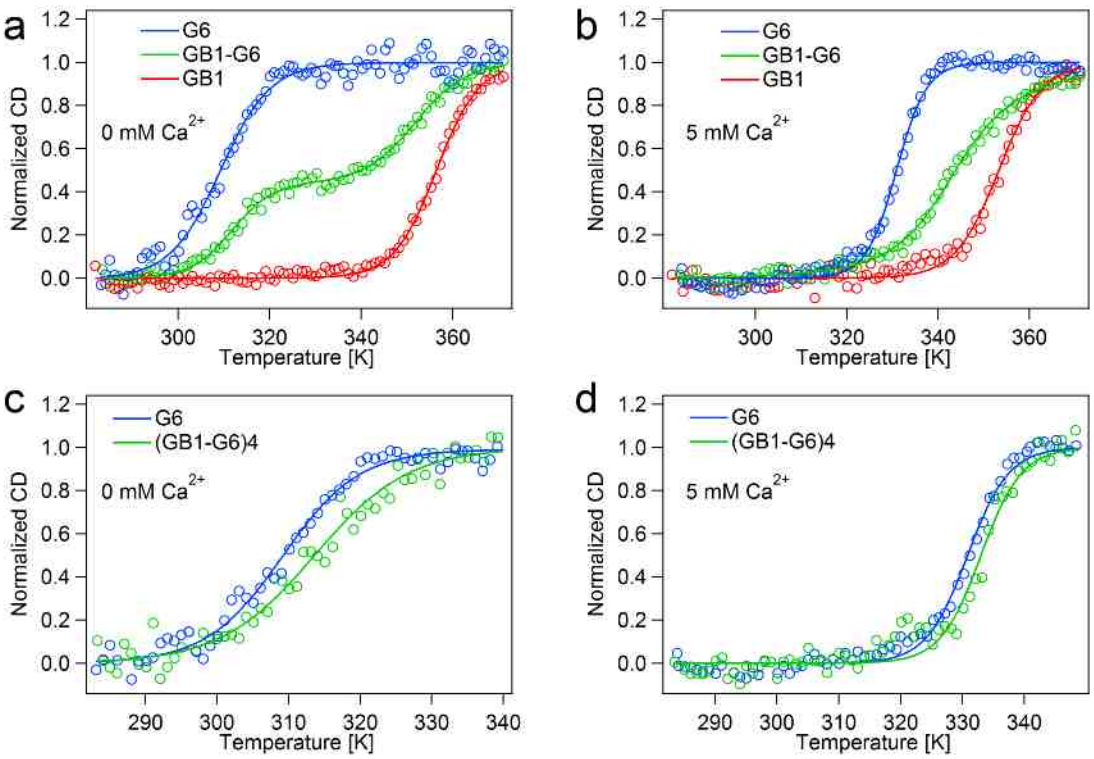

Supplementary Figure 4 The thermodynamic stability of G6 is not affected by linking to GB1. Thermal melting traces of G6, GB1-G6, and GB1 in the absence of calcium ions (a) and presence of 5 mM calcium ions (b) monitored by the CD signal at 222 nm. Thermal melting of G6 in the monomer (c) or $(GB1\text{-}G6)_4$ (d) constructs in the absence or presence of 5 mM of calcium ions. Because $(GB1\text{-}G6)_4$ gradually aggregates at temperatures higher than 343 K, the melting temperature for GB1 cannot be measured accurately. Circles in all figures correspond to experimental data and lines correspond to fitting with a sigmoid model (or double-sigmoid model). The melting temperature (T_m) of G6 is ~311 K for G6 in the monomer, GB1-G6, and $(GB1\text{-}G6)_4$ constructs in the absence of calcium ions; and T_m is ~333 K for G6 in the presence of 5 mM of calcium ions. The change in the melting temperature of G6 in the presence of GB1 is less than 3 K for all constructs. Moreover, the melting temperature of GB1 also is unchanged when linked to G6.

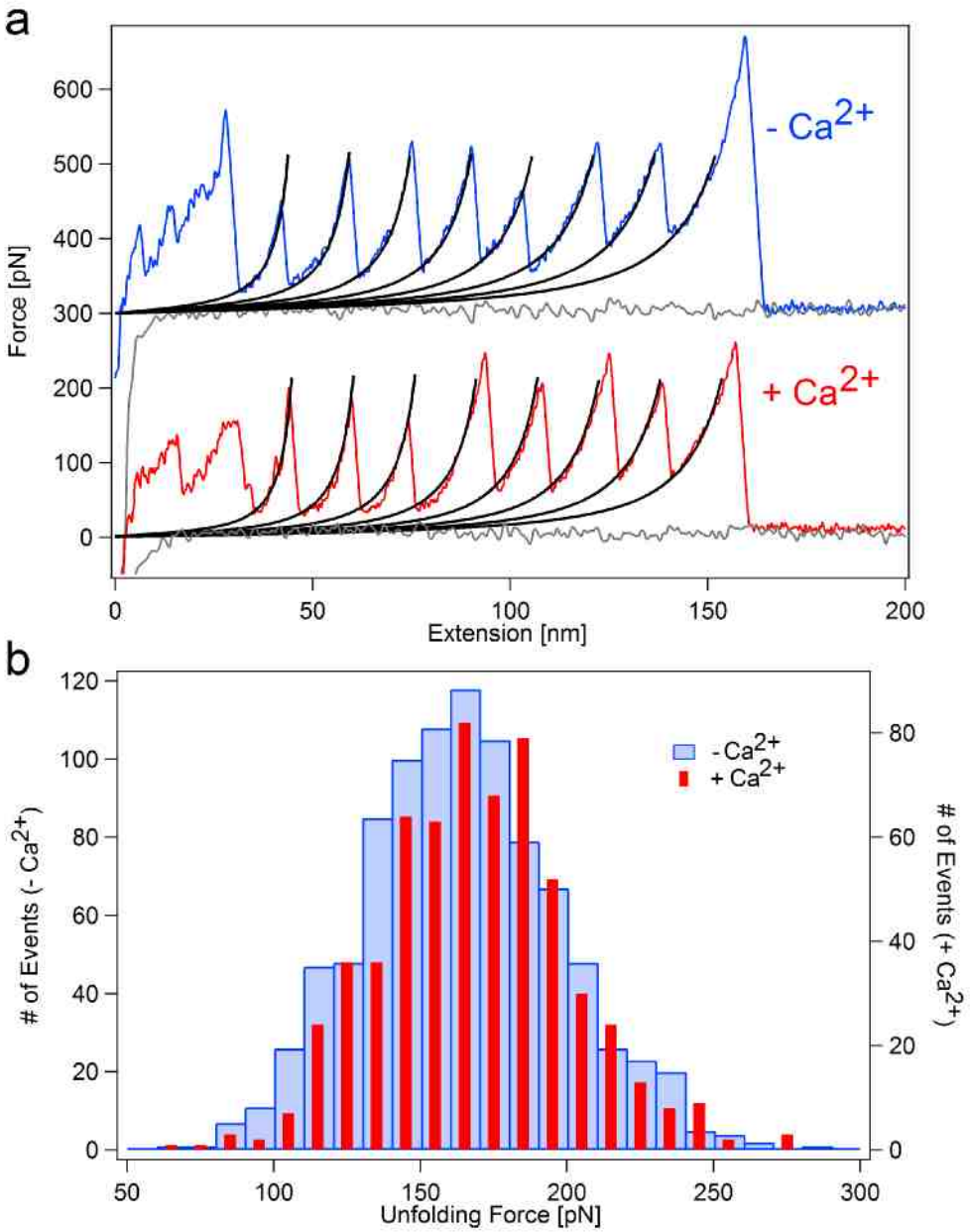

Supplementary Figure 5 The mechanical properties of GB1 are not affected in the presence of calcium ions. (a) Representative force-extension curves of the unfolding of $(GB1)_8$ at a pulling speed of 400 nm s^{-1} without (blue) and with (red) 5 mM of calcium ions. (b) The unfolding force histograms of $(GB1)_8$ without (blue) and with (red) 5 mM of calcium ions.

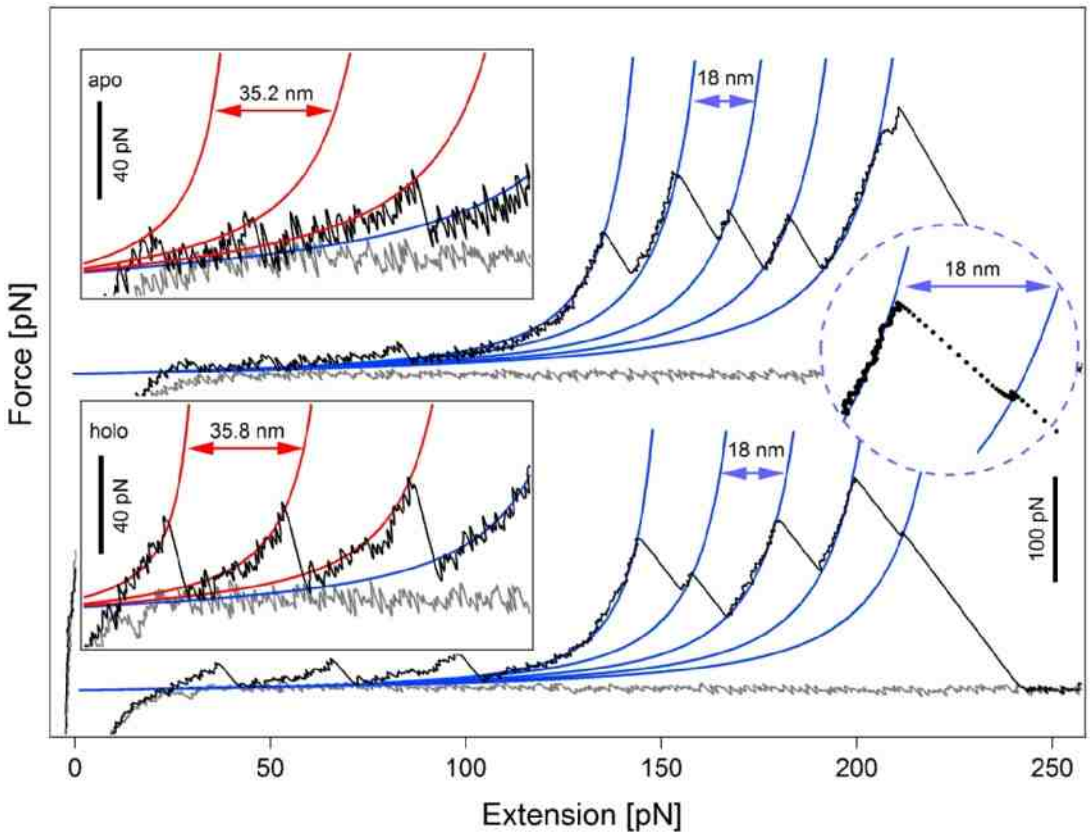

Supplementary Figure 6 Force-extension curves for $(GB1\text{-}G6)_4$ in the absence (top) and presence (bottom) of 50 μM calcium ions. The insets show enlarged regions corresponding to the unfolding of G6. Red and blue lines were fitted to force-extension curves using a worm-like chain model for polymer elasticity. The last peak of the bottom force-extension curve is also enlarged in the circle.

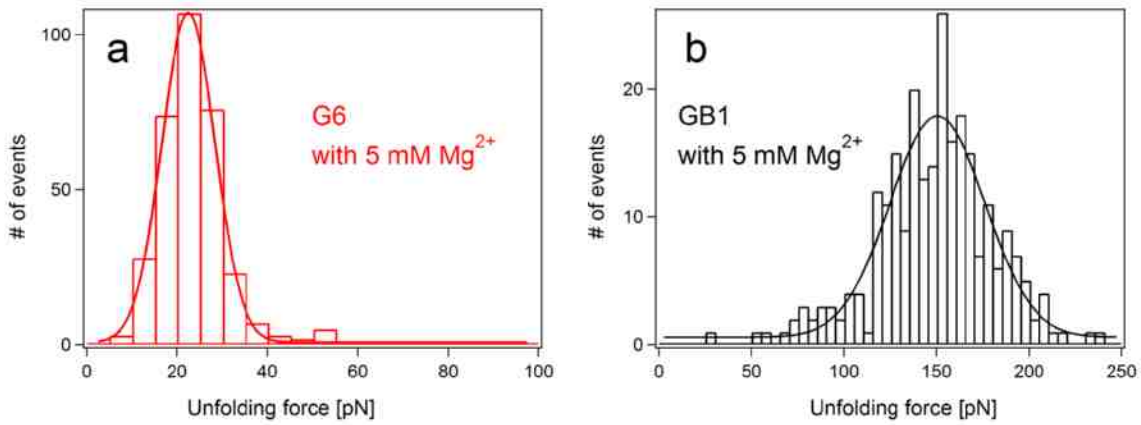

Supplementary Figure 7 Mechanical properties of G6 and GB1 with 5 mM magnesium ions. The unfolding force histograms for G6 (a) and GB1 (b) at 400 nm s^{-1} measured using polyprotein $(GB1\text{-}G6)_4$. Magnesium does not change the unfolding forces for G6 and GB1.

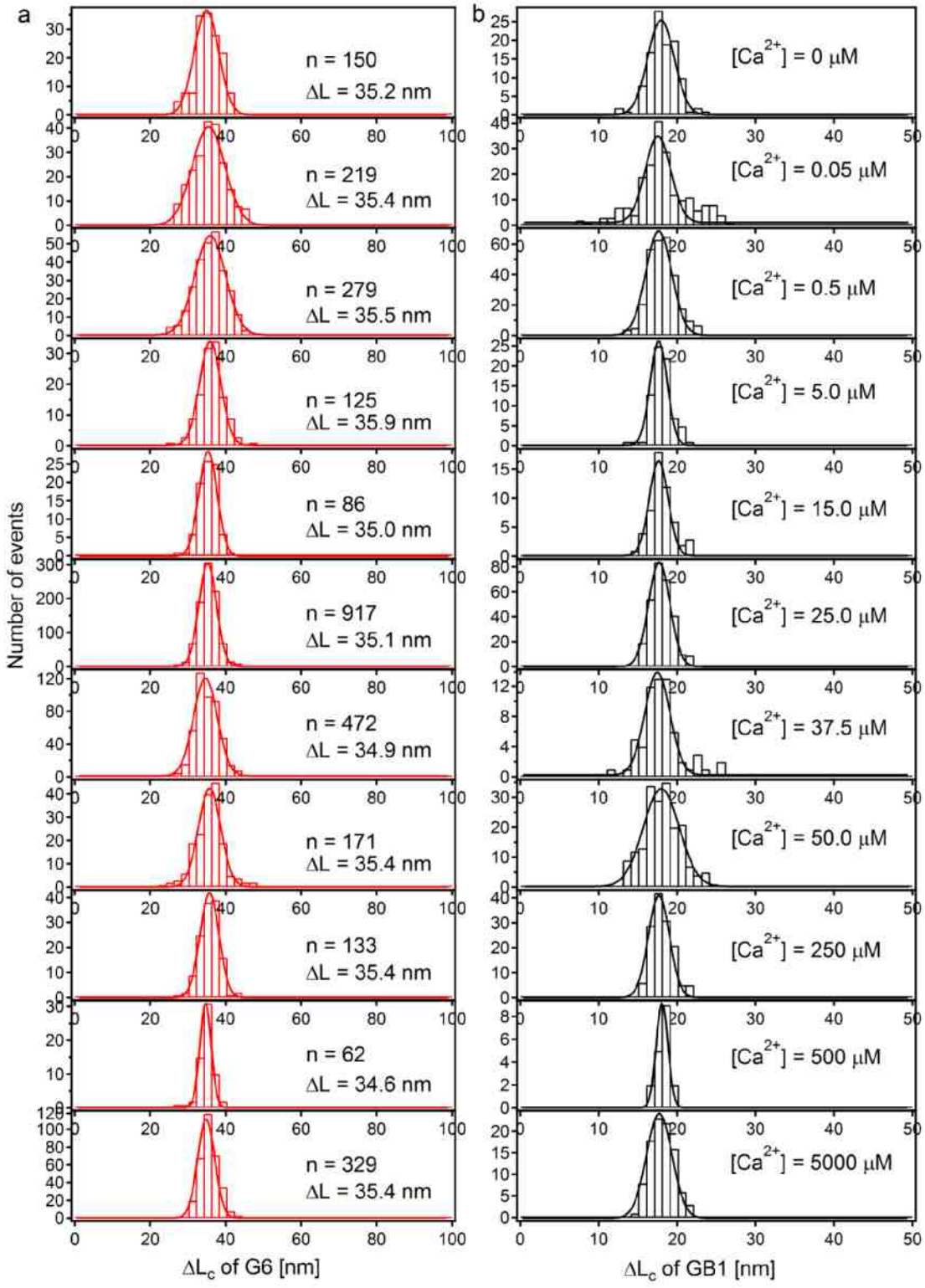

Supplementary Figure 8 Contour length increments of G6 and GB1 at different [Ca^{2+}]. (a) The contour length increments for G6. The number of G6 unfolding events and the average contour length increment of G6 are shown on the right side of each histogram of G6. The [Ca^{2+}]

are shown in the same row in (b). (b) The corresponding contour length increments of GB1at the same [Ca^{2+}]. The number of traces used for the histograms from top to bottom is 28, 59, 85, 38, 25, 293, 126, 49, 35, 15, and 107, respectively. We only selected traces containing at least three unfolding events of correct contour length increment for either GB1 or G6 for data analysis. Moreover, since GB1 serves as a fingerprint, for all selected traces, the unfolding force and the contour length increment for GB1 should be ~ 150 pN and ~ 18 nm, respectively. We used an auto data filtering program provided by JPK data acquisition software to reject all force-extension traces without any force peaks (including the detaching peak) higher than 30 pN. Therefore, only ~ 1-2% of the total traces are automatically collected and saved by the AFM setup. The rest were not collected because they do not contain any useful information. Among the collected traces, some traces arise from stretching multimeric molecules without the correct contour length increment for either GB1 or G6. Some of traces are too short with less than three unfolding peaks of GB1 or G6. These data account for ~ 2/3 of the collected traces and were not included in the data analysis. The contour length increment was the only criterion for data selection.

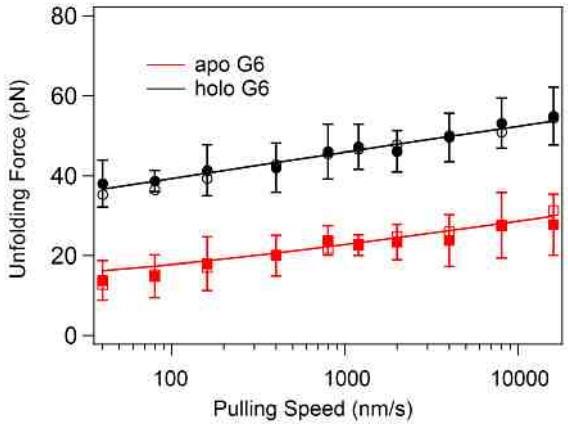

Supplementary Figure 9 Comparison of different data analysis methods. The unfolding force obtained using single molecule AFM experiments (solid circles and squares), Monte Carlo simulation (open circles and squares), and numerical fitting (continuous lines) are shown in the same figure. The detailed Monte Carlo simulation procedure has been reported elsewhere [1].

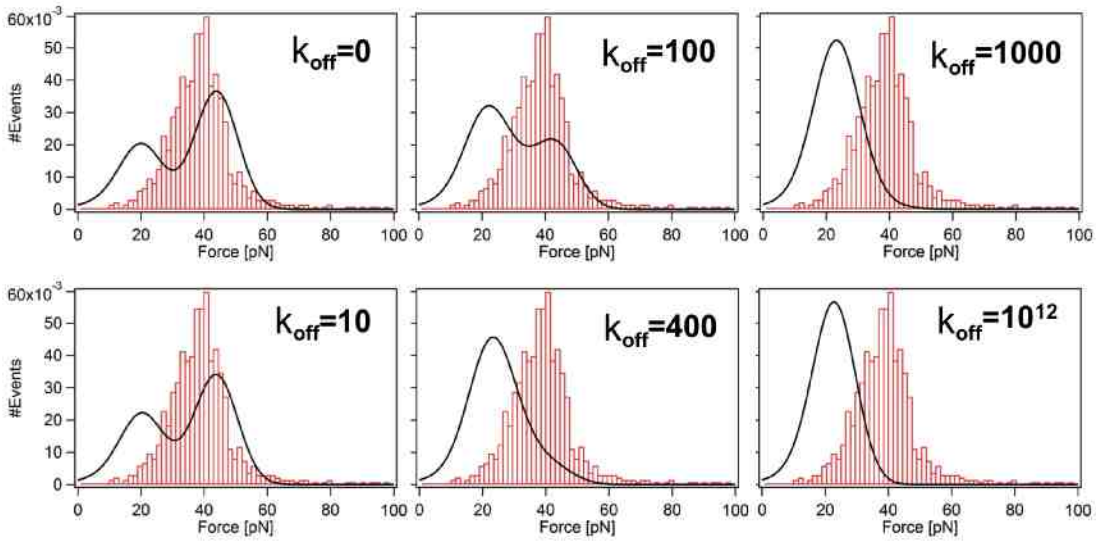

Supplementary Figure 10 The calculated unfolding force distributions by the force-independent binding model. Black lines correspond to the numerically calculated unfolding force distributions at a calcium concentration of 25 μM with various k_{off} rates shown on the top right corner of each figure and a fixed dissociation constant $K_d = k_{off}\,[Ca^{2+}]/k_{on} = 14.4\ \mu M$. Red histograms show measured data.

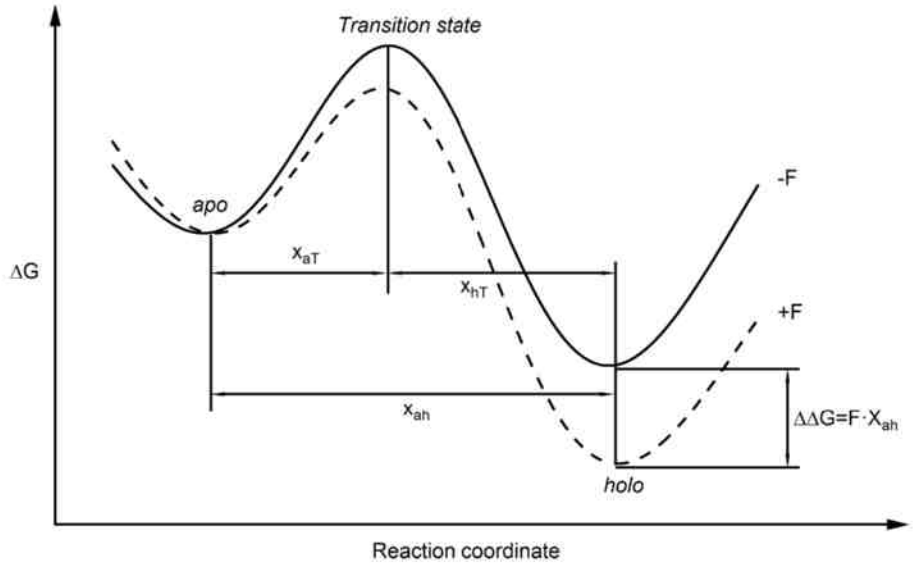

Supplementary Figure 11 A physical model for the effect of applied force on the inter-conversion of apo and holo states. We consider the apo and holo states are separated by a free energy barrier along the reaction coordinate, the direction of the applied force. The free energy landscape without applied force is shown by a solid line and that with applied force is shown by a dashed line, respectively. x_{aT} are x_{hT} are the distance of the transition state to the apo state and the holo state, respectively. These two parameters describe the dependency of forward and reverse exchange rate constants on the applied force. x_{ah} is the distance between the apo and holo states. The change of the relative free energy between apo and holo states equals $\mathbf{F}\cdot x_{ah.}$ Since $\Delta G=RTln(K_d)$, force changes the binding constant exponentially in this model.

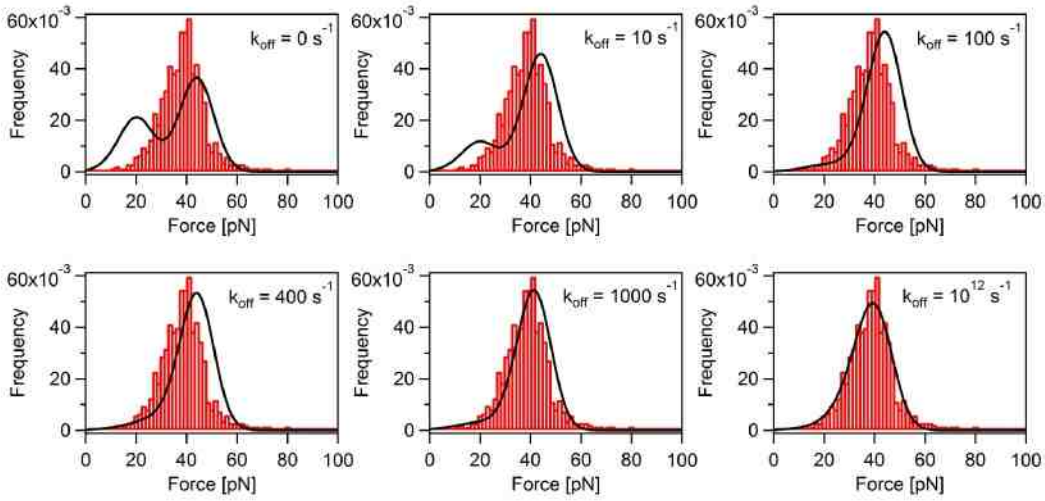

Supplementary Figure 12 The calculated unfolding force distributions by the force-dependent binding model. Black lines correspond to the numerically calculated unfolding force distributions at a calcium concentration of 25 μM with various k_{off} rates shown on the top right corner of each figure and a fixed dissociation constant $K_d = k_{off}[Ca^{2+}]/k_{on}$ = 14.4 μM. Red histograms correspond to the experimental data obtained by single molecule force spectroscopy.

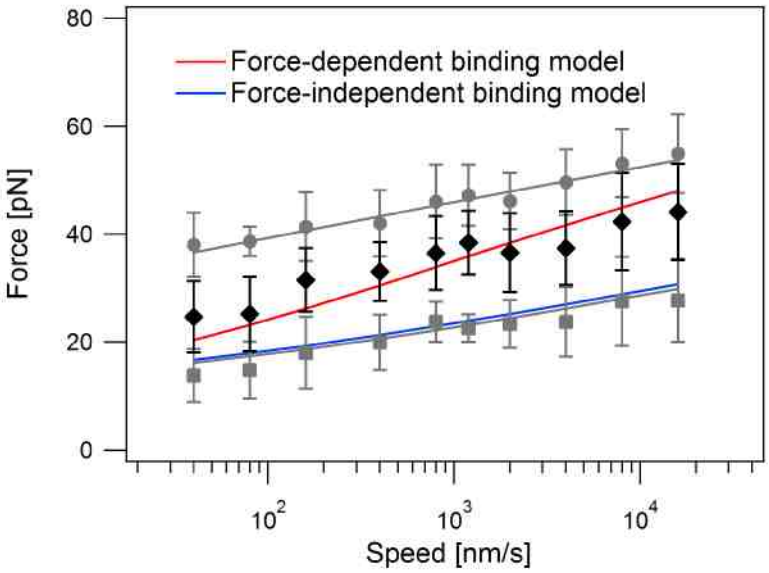

Supplementary Figure 13 Pulling-speed dependent unfolding forces for G6 at an intermediate [Ca^{2+}]. Black diamonds are the data in the presence of [Ca^{2+}] of 5 μM. The red and blue lines result from numerical fitting using the models described in the article. The pulling-speed dependent unfolding forces for apo and holo G6 (grey squares and circles, respectively) are also shown for reference.

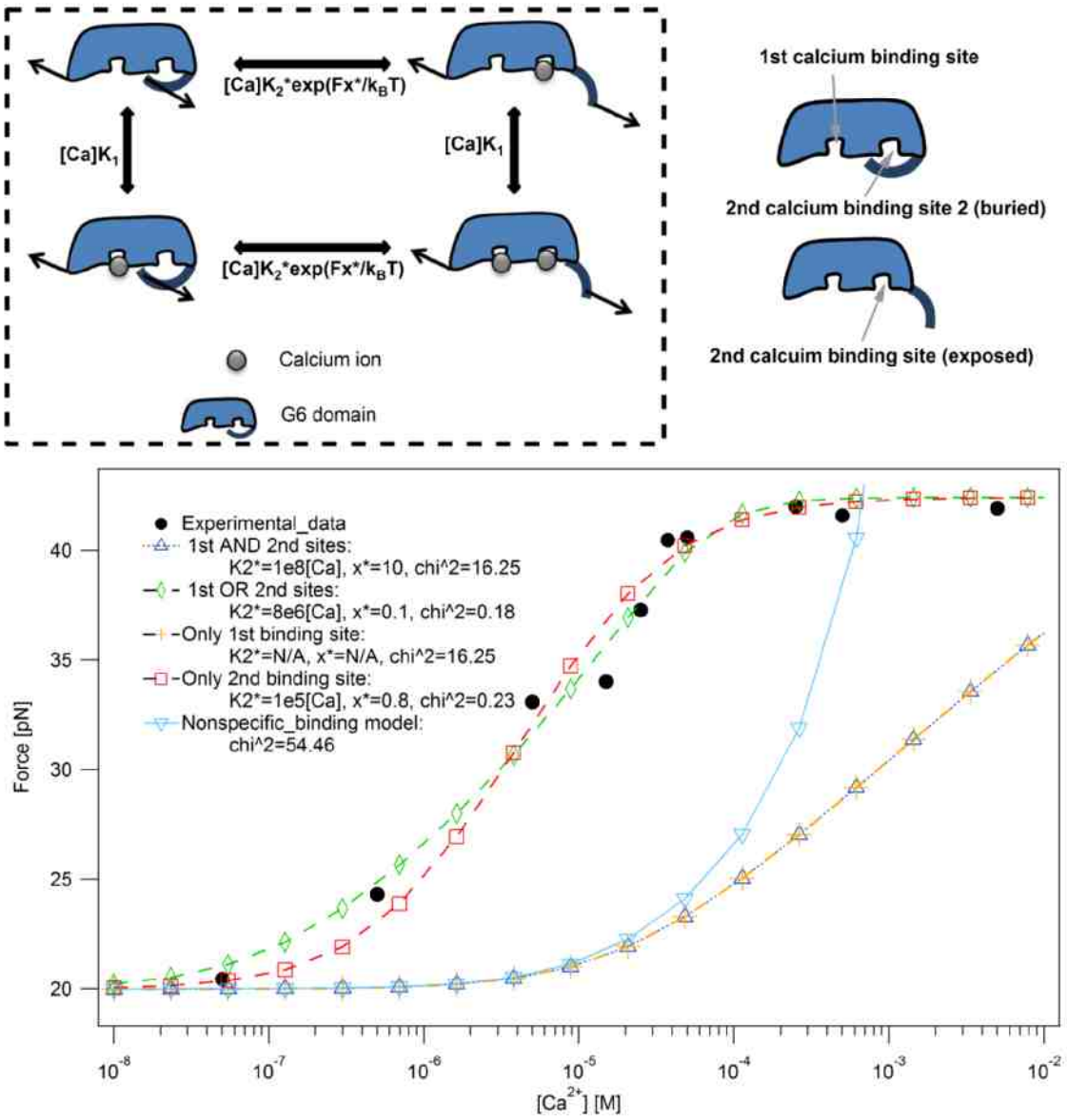

Supplementary Figure 14 Alternative models for the force-enhanced binding of calcium ions to G6. The first model considers the presence of an additional force-revealed calcium binding site. As shown in the scheme, the first binding site is exposed and the second binding site can be exposed by force. The equilibrium constants for inter-conversion among the four different states are shown by the double-headed arrows. The calcium binding affinity of the first calcium binding site is the same as that determined by ITC. Calcium binding affinities of the second site are listed in the lower figure after consideration of four different scenarios: i) The unfolding force for G6 is increased when both the first and the second sites are bound by calcium ions (blue triangles); ii) The unfolding force for G6 is increased when either the first or the second site is bound to a calcium ion (green diamonds); iii) Only the calcium binding to the first binding sites increases the unfolding force for G6 (orange crosses); iv) Only the calcium binding to the force-revealed (the second) binding site increases the unfolding force for G6 (red squares). The experimental data can be fitted reasonably well under scenarios ii and iv. The second model

considers non-specific binding of calcium to G6 (cyan inverted triangle). The free energy barrier for unfolding in the presence of calcium ions is $\Delta G(Ca^{2+}) = \Delta G_0 + m \cdot [Ca^{2+}]$, where ΔG_0 is the free energy barrier in the absence of calcium ions. We assume the increase in the free energy barrier is proportional to the calcium ion concentration, $[Ca^{2+}]$, with a slope, m. However, in this model, the unfolding force for G6 will not reach a plateau at high calcium concentrations, which contradicts the experimental observation.

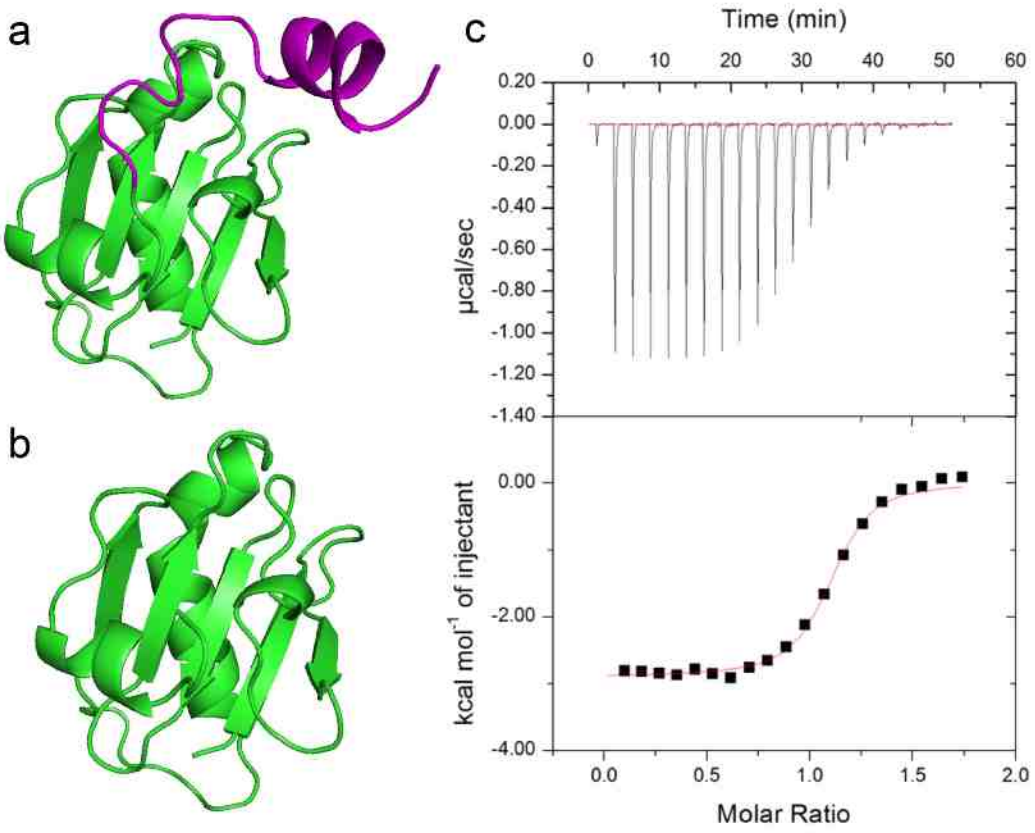

Supplementary Figure 15 The calcium binding affinity of G6 is enhanced when the C-terminal helix region is truncated. (a) The structure of apo G6. The G6 C-terminal extension region is highlighted in purple. (b) The structure of C-terminus truncated G6 (G6_cut). (c) The dissociation constant of calcium ion to G6_cut is 1.99 ± 0.25 µM, as measured by ITC. This indicates that the binding affinity of G6 is enhanced by 7-fold when the G6 C-terminal extension region is removed.

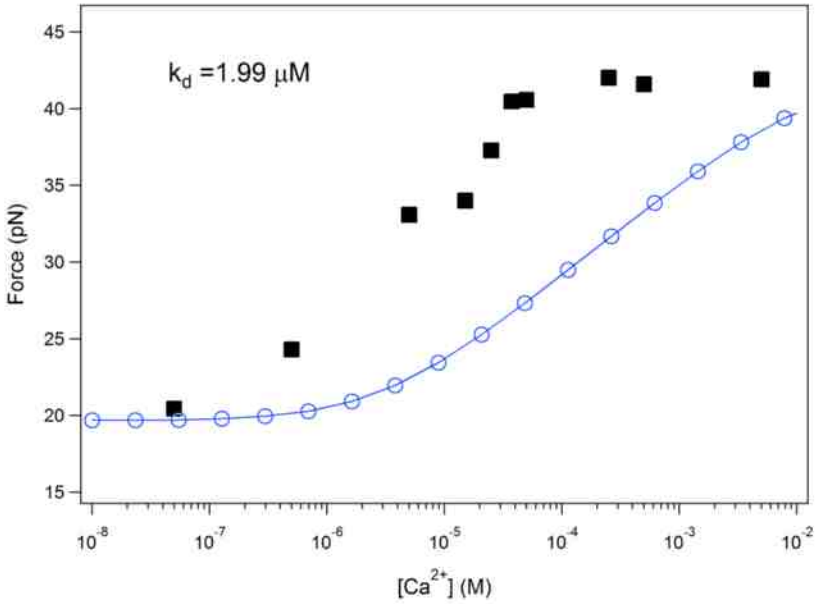

Supplementary Figure 16 Numeric simulation of the unfolding forces for G6. Simulation was done at different calcium concentrations using the force-independent model and the K_d of G6_cut (blue circles). Black squares are the experimental data.

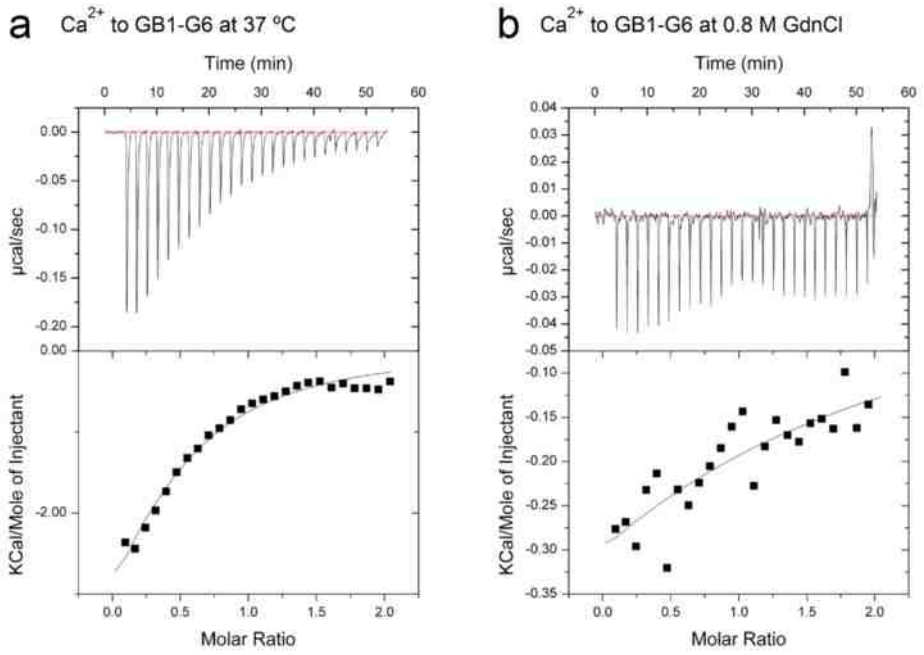

Supplementary Figure 17 The effects of temperature and chemical denaturant on the calcium binding affinity of G6. (a) The calcium binding affinity of G6 is decreased at an elevated temperature (37 °C). The K_d is ~ 56.2 µM for G6 at 37 °C. (b) The calcium binding affinity of G6 is decreased in the presence of chemical denaturant (0.8 M guanidinium chloride). The K_d is too low to be determined in 0.8 M guanidinium chloride.

Supplementary Methods

Numerical fitting of experimental data

1. Force unfolding kinetic equations

In the single molecule AFM experiments, Bell's expression was used to analyze the data. The rate constant for the unfolding of a protein in the presence of a time dependent external force, *F(t)* , is

$$k(t) = k_0 \exp\left[\beta F(t) x_t\right] \tag{1}$$

where k_0 is the spontaneous unfolding rate at zero force, x_t is the unfolding distance, namely, the distance from the free-energy minimum to the barrier, and $\beta = 1/k_B T$ (k_B is the Boltzmann constant and T is the absolute temperature). The external force can be described by worm-like-chain model of polymer elasticity as follows:

$$F(t) = \frac{1}{\beta p}\left[\frac{1}{4(1-\varphi)^2} - \frac{1}{4} + \varphi\right] \tag{2}$$

where p is the persistence length and $\varphi = vt/l_c$ (v is the pulling speed, t is time, and l_c is the contour length of the polyprotein chain). The probability of finding the protein in the folded state at time t, $p(t)$, is described by the equation of the two-state irreversible transition process:

$$\frac{dp}{dt} = -k(t)\, p \tag{3}$$

2. Force-independent model

In this model we assume that only apo and holo structures of G6 exist in the absence of force. Since the exchange rates between *apo* and *holo* states are not related to the external force, the dissociation constant K_d can be related to the forward and backward exchange rates, k_{ah} and k_{ha}, as:

$$k_{ah} / k_{ha} = (1/K_d)[\mathrm{Ca}^{2+}] \tag{4}$$

where $[Ca^{2+}]$ is the concentration of Ca^{2+}. The probabilities of the protein being in the apo state, p_a, and in holo state, p_h, satisfies the differential equation,

$$d\begin{pmatrix} p_a \\ p_h \end{pmatrix} / dt = \begin{pmatrix} -k_{ah} & k_{ha} \\ k_{ah} & -k_{ha} \end{pmatrix}\begin{pmatrix} p_a \\ p_h \end{pmatrix} \tag{5}$$

In the presence of external force on the gelsolin, both apo and holo states will irreversibly unfold to the denatured state. Then the above equation will be modified to a three state kinetic equation,

$$d\begin{pmatrix} p_a \\ p_h \end{pmatrix}/dt = \begin{pmatrix} -k_{ah} - k_a(t) & k_{ha} \\ k_{ah} & -k_{ha} - k_h(t) \end{pmatrix}\begin{pmatrix} p_a \\ p_h \end{pmatrix} \quad (6)$$

where k_a and k_h are the unfolding rate constants of apo and holo states of G6, which satisfy the Bell's equation as described before.

The probability of the distribution of lifetime of folded protein (in either the apo or holo states) at t equals to

$$-\dot{p}(t)dt = -\left(\dot{p}_a + \dot{p}_h\right)dt \quad (7)$$

The probability density of the rupture forces, dp/dF, is related to the probability density of lifetimes by

$$(dp/dF)dF = -\dot{p}(t)dt \quad (8)$$

The system of ordinary differential equations (equation 6) is solved by numerical integration with the Bulirsch-Stoer method or BDF method. (Igor Pro, Wavemetrics).

The convolution of the distribution of rupture force and the thermo noise, which is Gaussian white noise with a sigma of 6 pN, was used to fit the original data.

3. Modified force-dependent model

When force intervenes in the inter-conversion of apo and holo states, the kinetic equation (equation 6) should be modified. The exchange rate constants, k_{ah} and k_{ha}, become force-dependent variables instead of force-independent constants described in previous model. We assume that there is an energy barrier between apo and holo states (Supplementary Figure 11) as an analogy of Bell's model (Scheme S1). The rate constants of calcium binding (k_{ah}) and unbinding (k_{ha}) are determined by the activation energies (ΔG) and reaction lengths (x). The force-dependent rate constants are given by

$$k_{ah}(F) = A\exp[-(\Delta G_{aT} - F\cdot x_{aT})/k_BT] \quad (9)$$

$$k_{ha}(F) = A\exp[-(\Delta G_{hT} - F\cdot x_{hT})/k_BT] \quad (10)$$

where A is the attempt frequency in the Arrhenius equation and x_{aT} *and* x_{hT} are the distances over which force must be applied to reach the transition state from the apo and holo states, respectively. k_B and T are the Boltzmann constant and the absolute temperature, respectively. At zero force, $k_{ah0}=A\exp(-\Delta G_{aT})$ and $k_{ha0}=A\exp(-\Delta G_{aT})$. Therefore, the rate constant at a given time t can be written as

$$k_{ah}(t) = k_{ah0}\exp\left[\beta F(t)x_{aT}\right] \quad (11)$$

$$k_{ha}(t) = k_{ha0}\exp\left[\beta F(t)x_{hT}\right] \quad (12)$$

Therefore,

$$K_d(t) = k_{ha}(t)\cdot[Ca^{2+}]/k_{ah}(t) = K_{d0}\exp[\beta F(t)x_{ah}] \quad (13)$$

where $K_d(t)$ is the dissociation constant at time t, and $x_{ah} = x_{hT}\text{-}x_{aT}$.

Thus the kinetic equations for the protein unfolding under external forces are as follows:

$$d\begin{pmatrix} p_a \\ p_h \end{pmatrix}/dt = \begin{pmatrix} -k_{ah}(t)-k_a(t) & k_{ha}(t) \\ k_{ah}(t) & -k_{ha}(t)-k_h(t) \end{pmatrix}\begin{pmatrix} p_a \\ p_h \end{pmatrix} \quad (14)$$

The unfolding force distribution can be calculated using equations 7 and 8 with a similar procedure described for the force-independent model.

Although there are 5 fitting parameters in the force-independent model and 6 in the force-dependent one, these parameters are not independent free parameters. For the force-independent binding model, 4 fitting parameters related to the unfolding kinetics of apo and holo G6 (k_{ua0}, k_{uh0}, Δx_{ua} and Δx_{uh}) were predetermined from the pulling speed-dependent experiments shown in Figure 1 and set fixed in this model. The dissociation constant (K_d) of G6 was also predetermined from the ITC measurement and set as fixed in this model. Essentially, there is no free parameter in this model except for k_{off}. k_{off} is set arbitrarily (>1000 s^{-1}) to make sure the unfolding forces show a unimodal distribution (see Supplementary Fig. 11 for details.). Similarly, for the force-dependent binding model, these 5 parameters (k_{ua0}, k_{uh0}, Δx_{ua}, Δx_{uh} and K_d) were predetermined and set as fixed. The only free parameter is the x_{ah}, which describes how the dissociation constant is dependent on the applied force.

Estimation of the intramolecular force in the activated gelsolin.

The intramolecular force is estimated based the gelsolin-F-actin binding model proposed by Robinson *et al.*[2]. The loop between G3 and G4 contains 41 amino acids (373-413). The total contour length is *41aa * 0.365 nm/aa = 14.965 nm*. The end-to-end distance of this link in the proposed model is 6.6 nm. Based on the worm-like chain model for polymer elasticity,

$$F = \frac{k_BT}{p}\left(\frac{1}{4(1-x/Lc)^2}-\frac{1}{4}+x/Lc\right) = \frac{4.1pN\cdot nm}{0.4nm}\left(\frac{1}{4(1-6.6/14.965)^2}-\frac{1}{4}+6.6/14.965\right) = 10.16pN.$$

Here, the extension, x = 6.6 nm; the contour length, Lc =14.965 nm; k_BT = 4.1 pN·nm at 298 K; and p = 0.4 nm for unstructured polypeptide chain.

Isothermal titration calorimetry (ITC) measurement

ITC measurements were carried out on a MicroCal™ Isothermal Titration Calorimeter iTC200(GE Healthcare) in Hepes buffer (80 mM, containing 100 mM NaCl, and 2 mM EGTA, pH 7.5). The protein samples were dialyzed in the Hepes buffer with a final concentration of 40-100 μM. The calcium solutions were prepared in the same buffer and total calcium concentrations

were calculated by using WEB-MAXC (http://maxchelator.stanford.edu/). All solutions were degassed by being spun at 10,000 × g. for 15 min. To measure the binding constant, calcium solutions were injected into the calorimeter cell containing the protein solutions with 20 injections. The titration data and binding plots were analyzed using MicroCal Origin software with the one-site binding model.

Circular dichroism (CD) measurement

The far-UV CD spectra were obtained using a Jasco J-815 spectrophotometer (Tokyo, Japan) under constant nitrogen flushing at 25 °C. The protein concentration was ~0.2 mg mL^{-1} and the bandwidth was set to 1 mm. The contribution from the buffer (10 mM Tris) was subtracted. For each measurement, five scans were taken and averaged to increase the signal-to-noise ratio. In the varying temperature experiments, the change in θ_{MRE} at 222 nm was chosen to monitor the thermal melting of proteins. The temperature was increased from 4 °C to 90 °C with a ramp rate of 4 °C min^{-1}.

Supplementary References

[1] Gao, X., Qin, M., Yin, P., Liang, J., Wang, J., Cao, Y. & Wang, W., Single-molecule experiments reveal the flexibility of a Per-ARNT-Sim domain and the kinetic partitioning in the unfolding pathway under force. *Biophys. J.* **2012**, *102*, 2149-2157.

[2] Robinson, R. C. *et al.* Domain movement in gelsolin: a calcium-activated switch. *Science* **286**, 1939-1942 (1999)